Iranian Journal of Chemical Engineering
Vol. 16, No. 2 (Spring 2019), IAChE

Segregation Patterns of an Equidensity TiO_2 Ternary Mixture in a Conical Fluidized Bed: CFD and Experimental Study

M. Rasteh

Department of Chemical Engineering, Hamedan University of Technology, P. O. Box: 65155-579, Hamedan, Iran

ARTICLE INFO

Article history:
Received: 2018-08-29
Accepted: 2019-04-08

Keywords:
Fluidized Bed,
CFD Simulation,
Multi Fluid Model,
Ternary Mixture,
Segregation

ABSTRACT

In this study, an Eulerian-Eulerian multi-fluid model (MFM) was used to simulate the segregation pattern of a conical fluidized bed containing ternary mixtures of equidensity TiO_2 particles. Experimental 'freeze–sieving' method was employed to determine the axial mass fraction profiles of the different-sized particles and validate the simulation results. The profiles of mass fraction for large-, medium-, and small-sized particles along the bed height during the simulation time indicated that the particles' segregation could be predicted by CFD model. Effect of superficial gas velocity on segregation pattern was also investigated. It was shown that for $U_0=1.2U_{mf}$, partial segregation of large particles occurred, while for $U_0=1.6U_{mf}$, small- and medium-sized particles also segregated and full segregation was achieved. By increasing U_0 to $2U_{mf}$, mixing of different sized particles increased and particles segregation reduced. Therefore, it can be concluded that there was a critical velocity below which particles would segregate while above which their mixing increased.

1. Introduction

Fluidized beds are among the historically important unit operations that utilize gas-solid flows owing to their excellent mixing of the two phases, uniform concentration/temperature profile within the bed, and favorable heat and mass transfer characteristics [1,2]. In spite of the extensive occurrence of fluidized beds in different industries, some common phenomena such as the influence of polydispersity on system performance remain poorly understood [3,4].

Polydispersity (different particle sizes/densities) not only influences the bulk behavior of gas-solid fluidized beds, but may also lead to de-mixing of the particles called segregation [1]. In segregation phenomenon, larger/heavier particles behave as 'jetsam' and migrate to the bottom of bed, whereas smaller/lighter particles behave as 'flotsam' and are preferably accumulated in the top section of the bed [5]. In the cases where smaller particles have a higher density than their larger counterparts, a phenomenon called "inversion segregation" occurs. Inversion occurs when the small particles, which sink near the bottom of the bed at low gas velocities, migrate upward to the bed

* Corresponding author: mrasteh@hut.ac.ir

surface as the gas velocity increases [6].

Several competing parameters such as gravity, gas-phase turbulence, drag force, and particle interactions influence the final segregation state of a polydispersed mixture. Van Wachem et al. [7] showed that the predominant forces causing segregation were different depending on the superficial gas velocity. At low velocities, the main force is the drag, whereas increasing the gas velocity brings about increasingly important effects of gradients on granular temperature and pressure.

Segregation is a complex phenomenon that may be profitable or unfavorable depending on the application. For instance, segregation is needed in classifiers [8], while mixing is desired in the pharmaceutical industry to ensure that drug particles do not separate from ingredients before tableting [9]. Therefore, the segregation and mixing behavior in fluidized beds containing polydisperse mixtures should be thoroughly investigated for accurate design, proper operation, and efficient control of such systems.

Different aspects of particle segregation in fluidized beds have been widely investigated experimentally and numerically during the past several decades covering segregation mechanisms, possible incompatibilities and patterns, feasibility analysis, applications, and other associated specifications [10]. The common numerical methods are based on Eulerian-Lagrangian (discrete element model, DEM) and Eulerian-Eulerian (multi-fluid model, MFM) models via computational fluid dynamics (CFD) simulations [11]. The Eulerian–Lagrangian approach has the advantage of accounting for the corpuscular nature of particles by explicitly evaluating their trajectories. The disadvantage, however, is the high computational cost that increases with the number of particles. The main advantage of the MFM is that it requires a modest computational effort [12]. However, it is well known that its performance depends on the proper description of all possible intra- and inter-phase interactions, such as gas-solid interactions, collision, and frictional interactions between particles and also particles and wall [13].

Among the numerous CFD simulations of fluidized beds with polydisperse particles, binary mixtures have attracted much attention. Using the MFM approach, Huilin et al. [14] applied a kinetic theory of granular flow (KTGF) [15] for binary mixtures in their MFM simulations of a gas-fluidized bed containing particles with different sizes. The simulations showed that large particles accumulated near the distributor plate, as was also observed in corresponding experiments. Cooper and Coronella [16] conducted MFM simulation to study flow behavior of binary particles in a gas fluidized bed and showed segregation jump at a selected point in the bed. Applying both the MFM and DEM simulations, Huilin et al. [17] observed the particle segregation phenomenon in binary fluidized beds such that larger or heavier particles were settled near the bed bottom while relatively smaller or lighter particles, were found at the bed top. They also indicated that better particle mixing could be attained by increasing superficial gas velocity. Azizi et al. [18] conducted CFD simulation of particle segregation in bubbling gas-fluidized beds using an MFM simulation incorporating KTGF to study the fluidization behavior of a binary mixture of Geldart B particles at low gas velocities. Different drag models were tested to validate their model accuracy and it was shown that the Wen-Yu drag model was

the most appropriate for simulating size, density, and combined size/density segregations at lower gas velocities in bubbling fluidized beds. Chao et al. [19] used an MFM to investigate density segregation in a dense, binary fluidized bed. They studied the behavior of two types of particles with the same sizes but differing in density and, then, compared the results with experimental data from Formisani et al. [20]. Parametric studies of various operating and design variables of a bubbling fluidized bed were performed by Geng et al. [21] who studied the impact of important modeling parameters of solid wall boundary conditions, transport equations of granular temperature, particle-particle restitution coefficient, and the packing limit on the MFM results of a pseudo-2D bubbling fluidized bed. It was found that the predicted mixing behavior closely referred to the expression for granular temperature and also the specularity coefficient. Applying DEM, Feng et al. [22] simulated the flow behavior of flotsam and jetsam particles, and showed that the degree and rate of segregation were considerably affected by gas velocity and the final equilibrium states were not affected by the initial packing states for a given gas velocity. Effect of adding fine particles on segregation behavior of binary mixtures in gas-solid fluidized beds was studied by Norouzi et al. [23] through DEM simulation. The results showed that the addition of fines increased segregation of small- and large-sized particles by lowering inter-particle interactions, which resulted in enhanced mobility of larger particles.

In light of the literature survey, it was well understood that although the CFD/DEM and CFD/MFM simulations are commonly used for binary mixtures, there is a lack of CFD simulation for ternary particle mixtures focused on particle segregation pattern. Therefore, in the present work, a conical fluidized bed containing a ternary mixture of equidensity TiO_2 particles was simulated by multi-fluid model (MFM) via CFD simulation, and the dynamic and pseudo steady state segregation behavior of different sized particles was analyzed. The axial segregation pattern of ternary particles for different gas velocities was also discussed, and the simulation results of axial segregation profile were compared with the experimental data obtained by 'freeze-sieving' method.

2. Experimental procedure

The experiments were conducted in a conical fluidized bed made out of plexiglass, shown schematically in Fig. 1. Dimensions of the conical fluidized bed are given in Table 1. Gas distributor was a perforated plate with a standard mesh of 170. Air as fluidizing gas was supplied by a compressor (HSS make, model: MICAS-PH-80-1055, 1000 Lit/min) and entered into the bed after drying in two silica gel columns. Two rotameters with ± 2 % FSD accuracy for the lower ranges (0–5 m^3/h) and the higher ranges (5–20 m^3 /h) were placed in the air flow path to measure the air flow rates. Two pressure ports at the inlet (above the distributor) and outlet (at the exit section) of the bed were provided for recording the pressure drop along the bed height by a U-tube manometer, which used colored water as manometric fluid. The mass fraction of small-, medium-, and large-sized particles along the bed height was determined by a sieving shaker machine (AS200 control, Retsch GmbH, Germany) with sieves ranging from 1400 to 63 μm.

A ternary mixture of dried anatase titanium dioxide (TiO_2) particles composed of three particle sizes was used as the bed material and

filled in the bed in order to obtain the desired initial bed height (H_0=8 cm). The mixture with an average particle diameter of 170 micron is composed of three sets of mono-size particles with diameters of 85, 175, and 370 micron and weight fractions of 14 %, 63 %, and 23 %, respectively. The physical properties of TiO_2 particles are given in Table 2. In order to determine minimum fluidization velocity (U_{mf}), the investigation of characteristic curves ($\Delta P–U_0$) as a classical method for studying hydrodynamics of fluidization process was employed. This method was described in detail in [2] and, therefore, not repeated here for brevity.

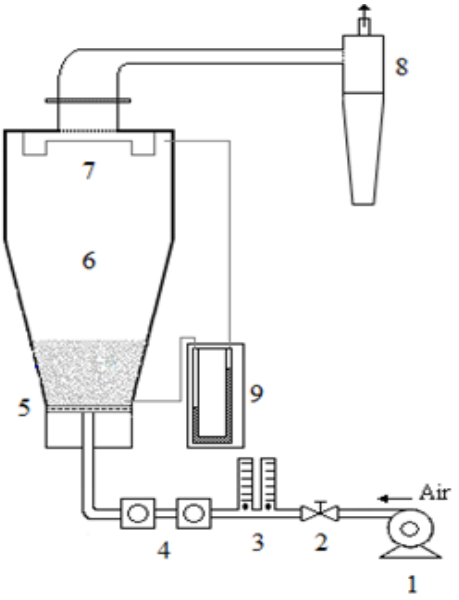

Figure 1. Experimental apparatus: 1. Air compressor, 2. Valves, 3. Rotameters, 4. Silica gel towers, 5. Gas distributor, 6. Conical fluidized bed, 7. Filters, 8. Cyclone, 9. Manometer.

Table 1
Geometry of conical fluidized bed in this study.

Dimension	Value
Bottom bed diameter	12 cm
Top bed diameter	24 cm
Cone angle	12°
Conical section height	18 cm
Cylindrical section height	30 cm
Total height of the bed	48 cm

Table 2
Physical properties of TiO_2 particles.

Property	Symbol (unit)	Value
Average particle size	$d_{p,avg}$ (μm)	170
Particle density	ρ_p (kg/m^3)	4500
Bulk density	ρ_b (kg/m^3)	2193
Total particle volume fraction	ε_s	0.65

To carry out axial segregation experiments, the bed was fluidized at a relatively high superficial gas velocity (U_0=2.5U_{mf}=0.135 m/s) for a time duration of 10 min to ensure perfect mixing and reproducibility of the initial condition for desired superficial gas velocities. After the end of mixing time, the air supply was shut off and, then, the bed was fluidized at the desired superficial gas velocities (U_0= 0.0648, 0.0864 and 0.108 m/s corresponding to 1.2U_{mf}, 1.6U_{mf}, and 2U_{mf}, respectively) for desired time (30 s). After the segregation time, the air flow rate was abruptly shut off to freeze the bed. The frozen bed was then divided into 8 sections along the bed height (1 cm apart), and the particles were vacuumed out of each section for sieve analysis and determining powder mass composition along the axial direction, as described in [3, 24].

3. CFD model description

The governing equations of MFM, simulation conditions, solution procedure, and initial and boundary conditions for hydrodynamic simulation of ternary mixture of TiO_2 particles in a lab-scale conical fluidized bed are explained in this section.

3.1. The Eulerian-Eulerian CFD simulation

In E-E or MFM, the gas and particulate phases behave as continuum fluid phases. That is, the phases act as interpenetrating continua, and the conservation equations in the form of generalized Navier-Stokes

equations are solved for each phase. Additional source terms are added to the conservation equations to account for the interactions between the phases. Kinetic theory of granular flow (KTGF), which makes an analogy between the particulate phases and the kinetic theory of gases, is used for evaluating the granular temperature (kinetic energy of particulate phase) and other particulate phase properties. The set of governing equations and consecutive models of the MFM and KTGF are presented in Appendix A. More detailed discussions about the governing equations may be found in [18,25,26].

Simulations have been performed in a Cartesian coordinate system using the bed geometry given in Table 1. The gas and particulate phase's specification and also simulation parameters are summarized in Tables 3 and 4.

Table 3
Physical properties of four phases used in simulations.

		Property	Value
Gas: air (primary phase)	phase 1	density (kg/m^3)	1.225
		viscosity (pa.s)	1.785×10^{-5}
		Pressure (atm)	1
Particles: TiO_2 (secondary phase)	phase 2	particle diameter (μm)	85
		particle density (kg/m^3)	4500
		bulk density (kg/m^3)	2208
		solid volume fraction	14 %
	phase 3	particle diameter (μm)	175
		particle density (kg/m^3)	4500
		bulk density (kg/m^3)	2201
		solid volume fraction	63 %
	phase 4	particle diameter (μm)	370
		particle density (kg/m^3)	4500
		bulk density (kg/m^3)	2193
		solid volume fraction	23 %

Table 4
Simulation parameters.

Hydrodynamic model	Eulerian-Eulerian
Viscosity model	Standard k-ε
Drag models	Gidaspow
Particle–particle restitution Coefficient	0.95
Granular viscosity	Gidaspow
Granular bulk viscosity	Lun-et-al
Frictional viscosity	Schaeffer
Angel of internal friction	30^o
Friction packing limit	0.61
Solid pressure	Lun-et-al
Radial distribution	Lun-et-al
Maximum packaging limit	0.67
Specularity coefficient	0.9
Superficial gas velocities (based on bed bottom diameter)	0.0648 ($1.2U_{mf}$) , 0.0864 ($1.6U_{mf}$), 0.108 ($2U_{mf}$) m/s
Initial bed height	8 cm

3.2. Solution procedure

The CFD simulations were carried out by the commercial software package FLUENT 15.0.7 (Ansys Inc.) with a double precision option. The phase coupled SIMPLE algorithm was applied to pressure-velocity coupling under the transient condition. Least Squares Cell Based for gradient, Second Order Upwind scheme for momentum, turbulence kinetic energy, and turbulent dissipation rate were used for spatial discretization to obtain more precise results. Fixed option with a value of 10^{-4} for time step (after studying time step dependency) was used for transient simulations, and the value of 50 for maximum iteration per time step was set. To ensure relatively low error between two consecutive iterations, the convergence criterion of 10^{-3} was considered for all scaled residuals.

3.3. Boundary conditions

A no-slip boundary condition was applied to the gas phase at the wall, and Johnson and Jackson's [27] slip wall boundary condition (Appendix B) was used for the solid phase. The parameter φ in Johnson and Jackson boundary condition is called specularity coefficient, which varies due to roughness and shear at the wall. The value of 0.9 for specularity coefficient, corresponding to partial slip boundary condition, was used for solid phases in these simulations. At the inlet of the conical fluidized bed, the gas enters only in the axial direction (Dirichlet boundary condition), and superficial gas velocities of 0.0648, 0.0864, and 0.108 m/s were set as the inlet gas velocity. At the outlet of the bed, an outflow boundary condition was used, which means that the gas velocity gradient was set to zero along the axial direction ($\frac{\partial u_y}{\partial y} = 0$) and atmospheric condition for pressure was also imposed.

4. Results and discussion

4.1. Grid-size dependency analysis

Three structured meshes corresponding to the number of nodes equal to 17672 (94×188), 45000 (150×300), and 64800 (180×360) were created in order to study mesh dependence solution, and to ensure that the CFD simulation results are independent of the mesh size. Total bed pressure drop (ΔP) and bed expansion ratio (R) were selected as the overall hydrodynamic parameters for performing the grid dependency study, and the simulation results for different meshes were compared with the experimental data for the bed with an initial height of 8 cm and a superficial gas velocity of 0.0864 m/s. Fig. 2 shows that the simulation results for the fine (64800) and medium (45000) grid sizes for ΔP (Fig. 2-a) and R (Fig. 2-b) have no significant differences, while the results for the coarse grid (17672) show disparity with those of fine and medium grid sizes. The average size of cells in the medium grid size is about 11 times the average particle diameter, which is consistent with 10 to 12.5 times used in the earlier studies [28,29]. Average simulated values for ΔP and R (time averaged for duration of 20 <t<30 sec), relative errors compared to experimental data, and the CPU time required for simulation of one second of the bed motion with a computer equipped with CPU Core i7 6700K 4.0 Ghz, and RAM, 16 GB DDR4 are presented in Table 5. Accordingly, to provide sufficient accuracy with reasonable computational cost, in this study, the medium grid size is used for all simulations.

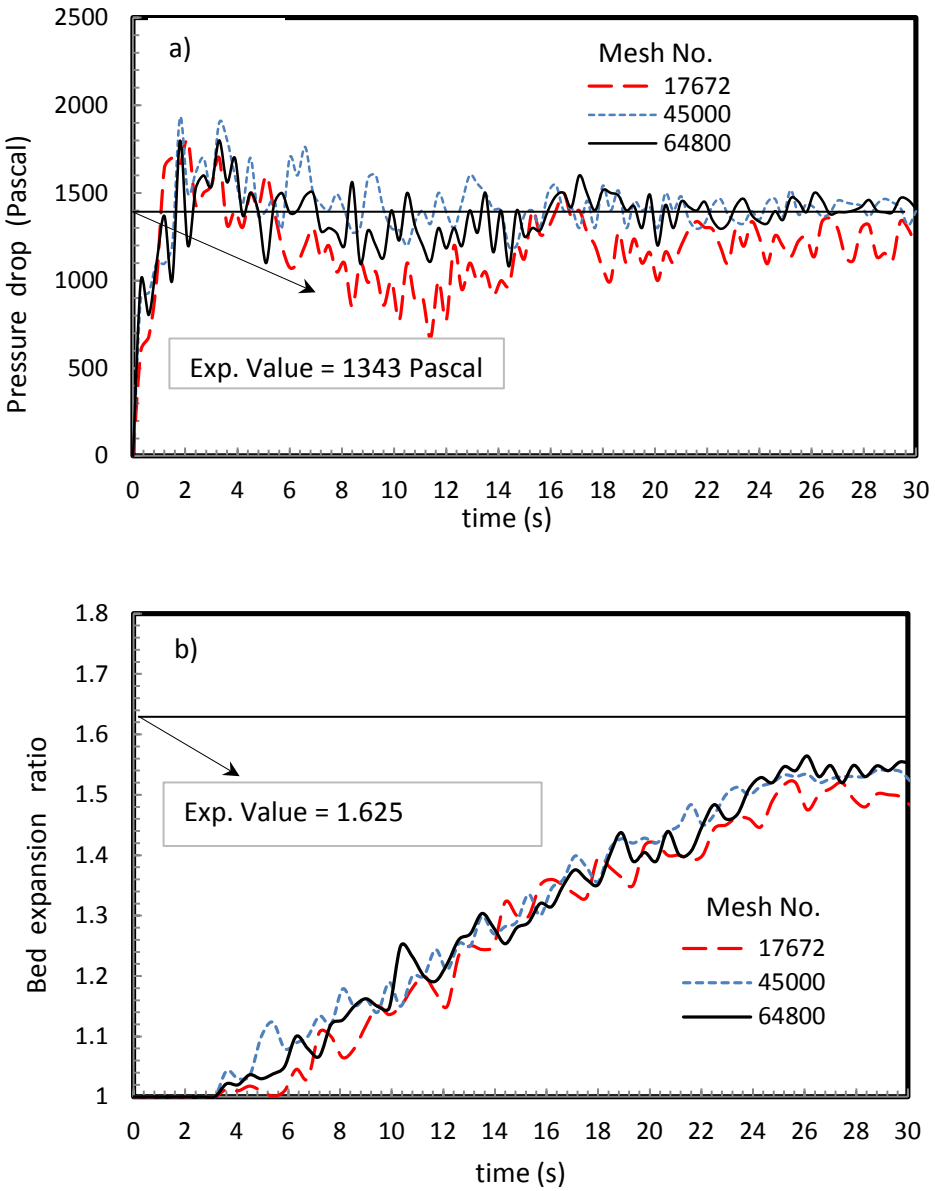

Figure 2. Total pressure drop (a) and bed expansion ratio (b) versus time for different mesh numbers. (U_0=0.0864 m/s and H_0= 8 cm).

Table 5
Average pressure drop, bed expansion ratio and required CPU time for different meshes.

Mesh number	Average of ΔP (Pascal) 20< t <30 sec	Relative error (%)	Average of R 20< t <30 sec	Relative error (%)	Required CPU time for 1 sec simulation (h)
17672	1220	-9.1	1.49	-8.5	4.11
45000	1415	5.4	1.52	-6.3	5.61
64800	1411	5.1	1.53	-5.9	7.25

4.2. Segregation pattern

Solid volume fractions of small-, medium-, and large-sized particles for superficial gas velocity 0.0864 m/s ($1.6U_{mf}$) at times=0, 10, 20, and 30s from the beginning of simulation are shown in Fig. 3. At t=0, the particles are

well-mixed; however, with time, the large particles are gradually accumulated in the bottom region of the bed, and the small particles are gathered in the top zone, while medium-sized particles appear in the middle region of the bed. This result is in agreement with the observation of Huilin et al. [14] who studied size segregation of binary mixture in bubbling fluidized beds. It is seen from Fig. 3 that at t=20 s, large particles almost segregate, while medium- and small-sized particles are still mixed; however, at t=30 s, the small- and medium-sized particles also separated and the complete segregation occurred. Contour plots of volume fractions of different size particles and also the total solid volume fractions are presented in Fig. 4. Segregation of large particles at t=20 s and full segregation of different size particles at t=30 s are observed from this figure. The observed segregation is consistent with pattern shown in Fig. 3.

The experimental results of the particles segregation obtained from the "freeze-sieving" method for a superficial gas velocity of 0.0864 m/s at t=20 and 30s are presented in Fig. 5. In the "freeze-sieving" method [4], the bed is fluidized for specific time duration and, then, is de-fluidized suddenly to "freeze", particles are vacuumed from each section of the bed height to determine the mass fraction of different particle sizes by sieving. As seen from Fig. 5a, at t=20s, the major part of the large particles is accumulated in the lower region of the bed, while the small and medium particles are mixed in the middle and upper parts of the bed. At t=30s (Fig. 5b), the small and medium particles also segregate so that they appear mainly in the upper and middle layers of the bed, respectively. The simulation results of the segregation analysis given in Figs. 3 and 4 are in good agreement with the experimental results presented in Fig. 5.

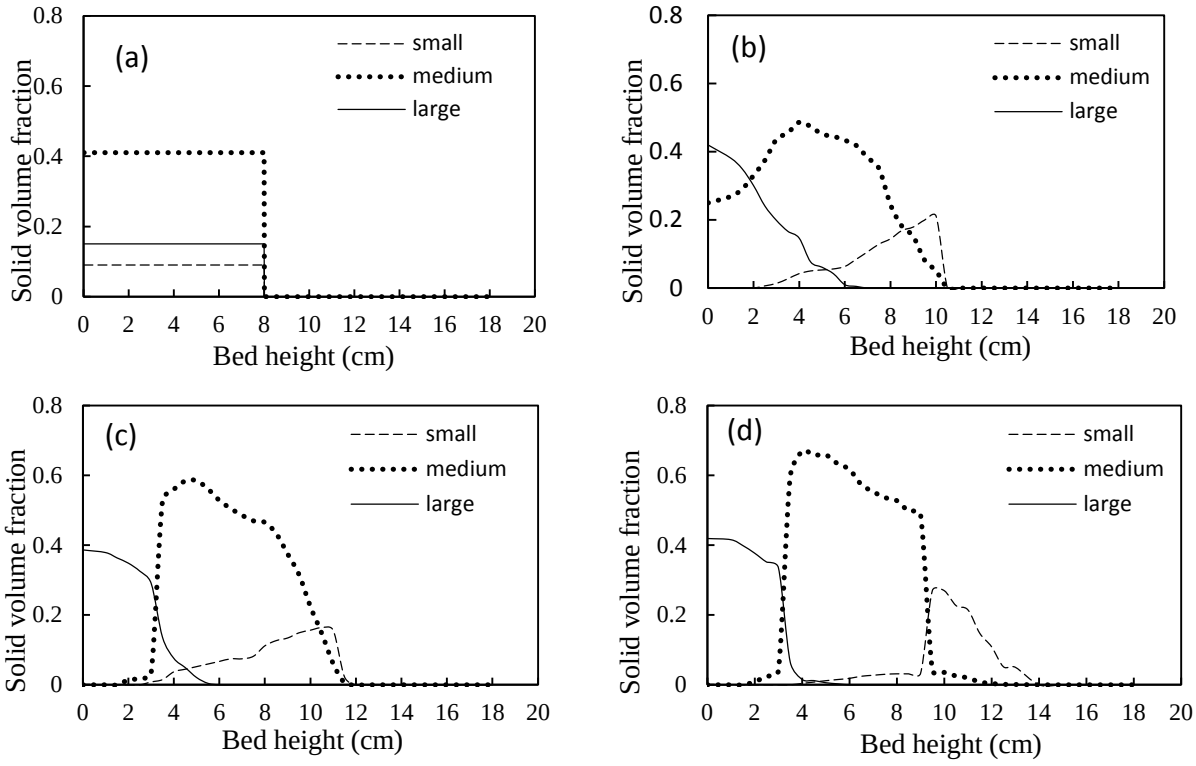

Figure 3. Segregation patterns of particle mixture at U_0=0.0864 m/s; (a: t= 0, b: t=10, c: t=20, and d: t= 30 sec).

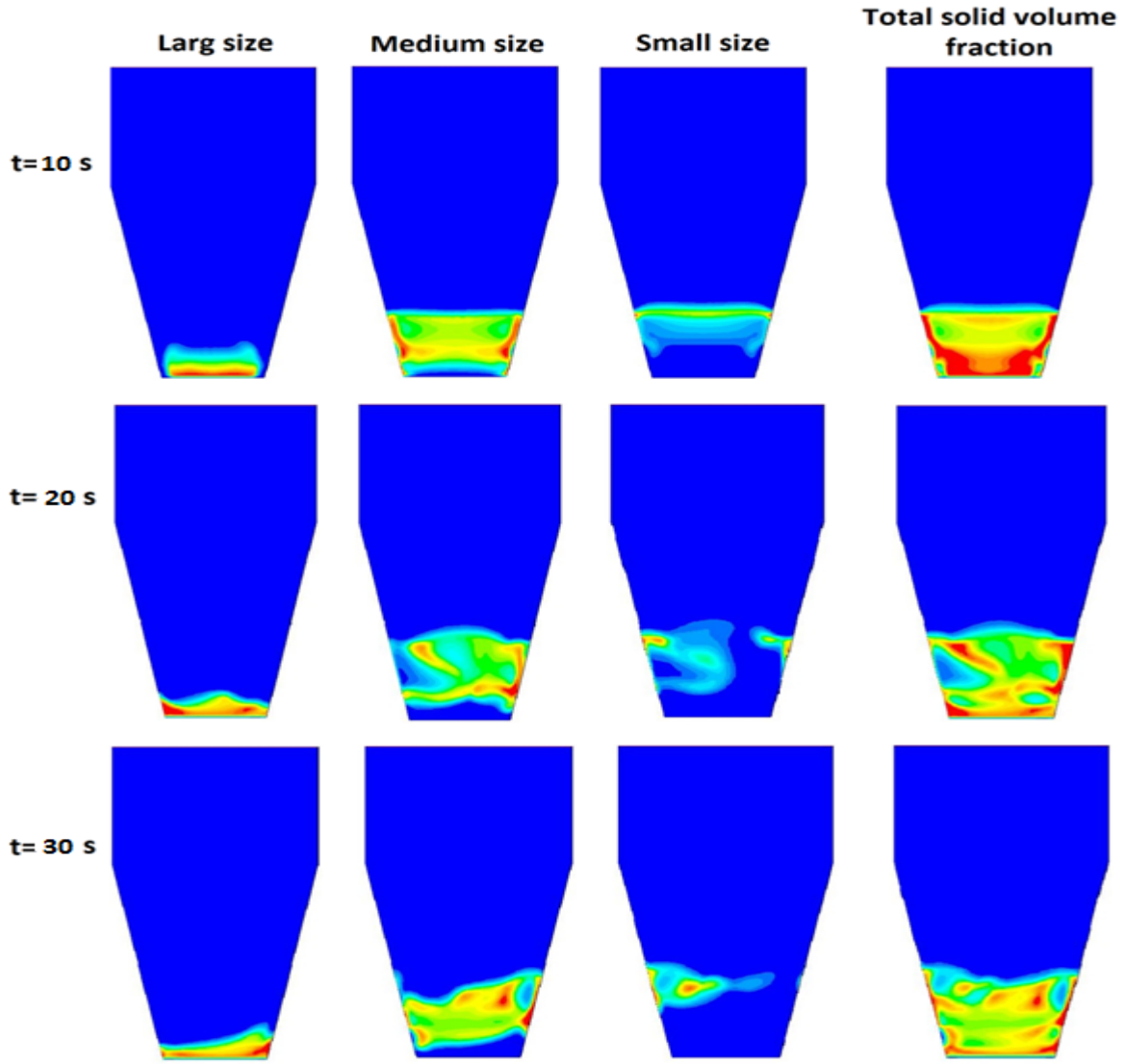

Figure 4. Contours of volume fractions of large, medium, and small particles and total solid volume fraction at U_0=0.0864 m/s.

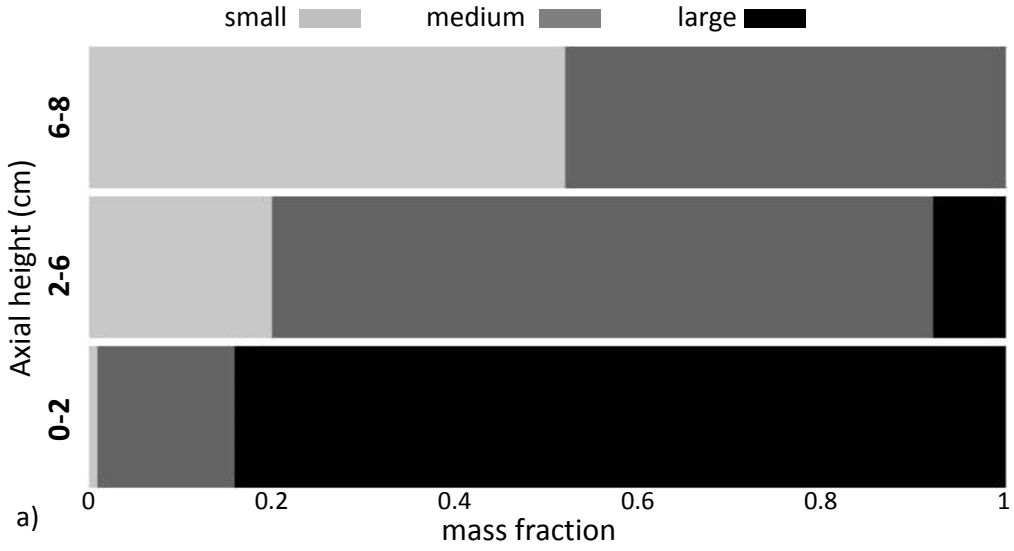

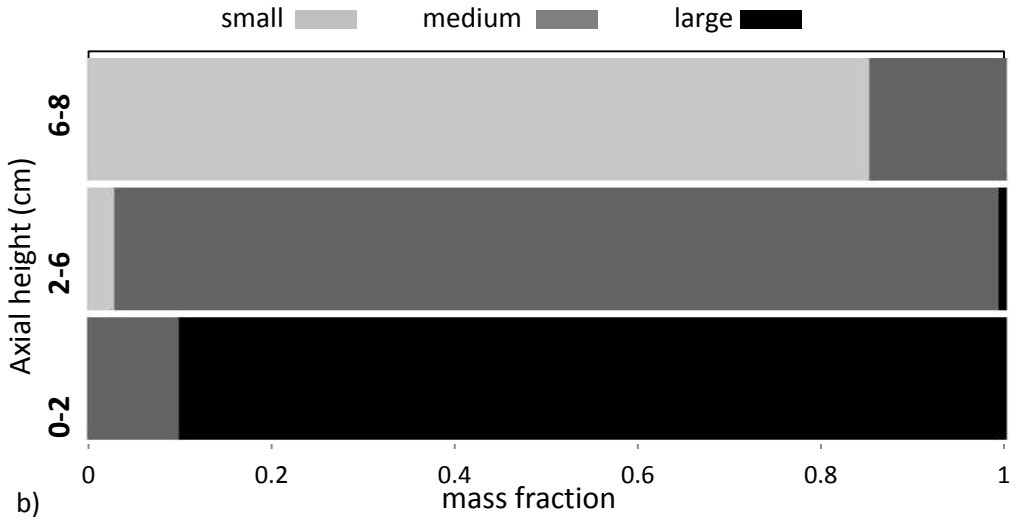

Figure 5. Weight fraction of different sized particles along the bed height at U_{mf}= 0.0864 m/s (a: t= 20 and b: t= 30 sec).

4.3. Effects of gas velocity on particle segregation

Fig. 6 shows the solid volume fraction contours for small-, medium-, and large-sized particles for different superficial gas velocities in the range of $1.2U_{mf}$ to $2U_{mf}$ (0.0648 to 0.108 m/s) at t=30s. As can be seen in Fig. 6a, for gas velocity $1.2U_{mf}$ (0.0648 m/s), large particles segregate and accumulate in the bottom region of the bed, while segregation of small and medium particles does not occur. For the gas velocity of $1.6U_{mf}$ (0.0864 m/s), the segregation of medium and small particles also occurs, leading to the complete segregation of the bed (Fig. 6b). With increasing superficial gas velocity from $1.6U_{mf}$ to $2U_{mf}$ (0.0864 to 0.108 m/s), the mixing of different size particles increases and particle segregation reduces (Fig. 6c). These results are in agreement with the observation of Zhang et al. [30], who studied particle segregation for binary system in a cylindrical fluidized bed. They found that there was a critical value for superficial gas velocity below which particles segregate; however, for high gas velocities, the particles are more mixed.

Simulation results of solid volume fraction profiles of small-, medium-, and large-sized particles along the bed axis for different superficial gas velocities in the range of $1.2U_{mf}$ to $2U_{mf}$ are presented in Fig. 7. It is seen that, for superficial gas velocity $1.2U_{mf}$, small- and medium-sized particles are distributed in the middle and upper regions (Fig. 7a-b); however, large particles reside only in the bottom region of the bed (Fig. 7c). This shows that, for this gas velocity, only the segregation of large particles occurs, while small and medium particles are still mixed. For gas velocity $1.6U_{mf}$, small, medium, and large particles are concentrated in the upper, middle, and bottom regions of the bed, respectively, indicating the full segregation of particles. It is observed from Fig. 7 that the solid volume fraction profiles of different size particles have become more uniform for the higher superficial gas velocities ($U_0 = 2U_{mf}$). Therefore, it can be concluded that the mixing of particles is intensified and particle segregation is reduced for gas velocities higher than 1.6 U_{mf}. These observations are consistent with the results shown in Fig. 6.

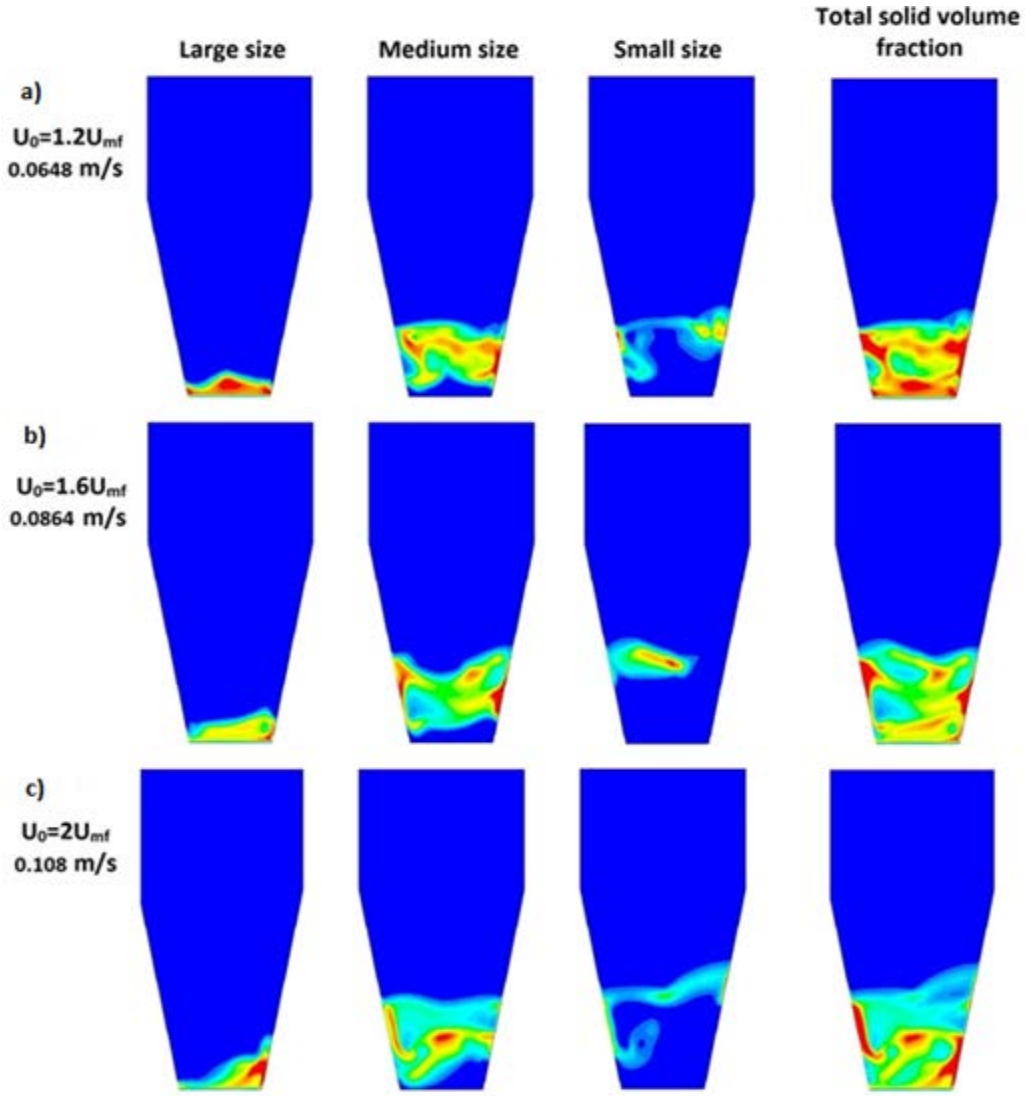

Figure 6. Contours of volume fractions of large, medium, and small particles for different superficial gas velocities.

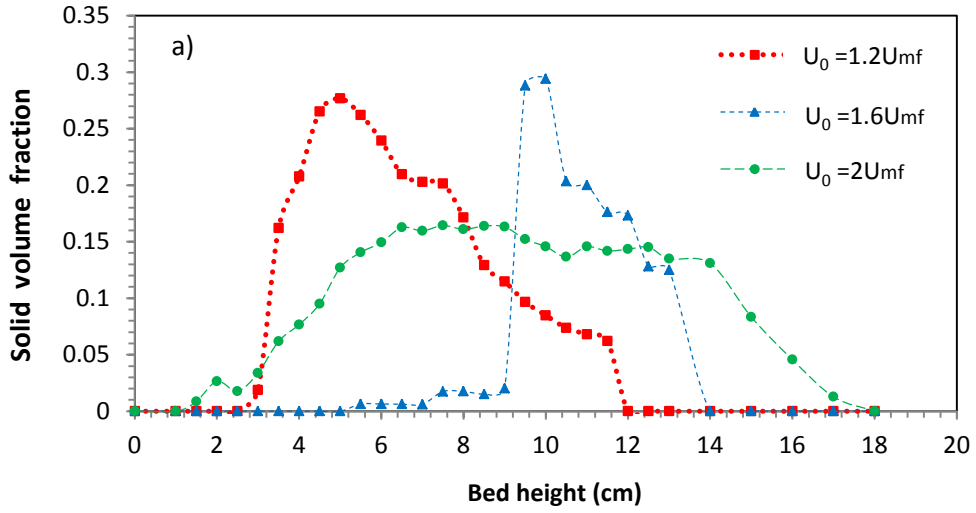

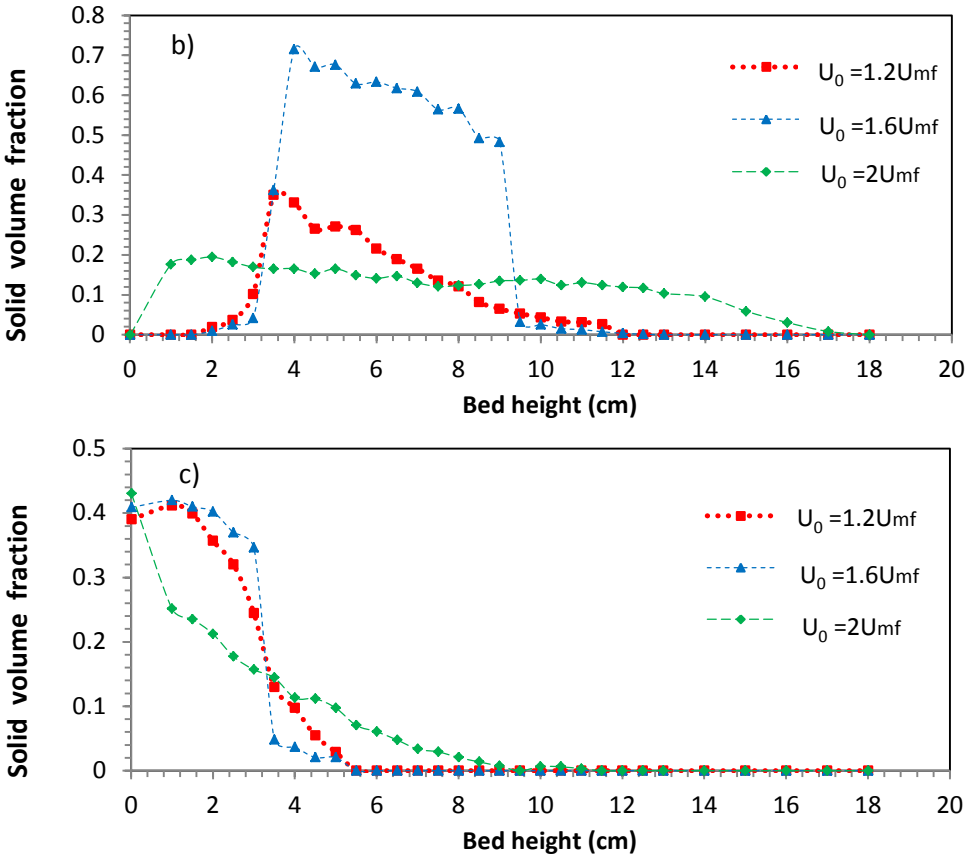

Figure 7. Solid volume fraction profiles of a) small, b) medium, and c) large particles versus bed height for different superficial gas velocities.

5. Conclusions

The segregation behavior of a conical fluidized bed containing ternary mixtures of equidensity TiO_2 particles was investigated by an MFM/CFD simulation. The characteristics of segregation were analyzed using the governing equations of multi-fluid model (MFM) and the constitutive correlations obtained from the kinetic theory of granular flow (KTGF).

The MFM model, predictions for the time evolution of solid volume fraction profiles of large-, medium-, and small-sized particles along the bed height were evaluated. The results showed that the partial segregation after t=20s and full segregation after t=30s were predicted by the MFM for the superficial gas velocity of $1.6U_{mf}$, which are in agreement with experimental results obtained from "freeze-sieving" method. When full segregation occurred, large particles settled to the bed bottom layers and small particles floated to the bed upper region. These two zones are separated by the third intermediate one, composed of medium-sized particles.

An examination of superficial gas velocity effects on particle segregation revealed that, for $U_0=1.2U_{mf}$, large particles were accumulated in the bottom region of the bed; however, small- and medium-sized particles were still mixed. For $U_0=1.6U_{mf}$, small- and medium-sized particles also segregated and full segregation occurred. For $U_0=2U_{mf}$, mixing of different size particles was increased and particles segregation was reduced. Therefore, it was concluded that different size particles would segregate at lower superficial gas velocities, while their mixing increased above a critical gas velocity.

Nomenclature

C_D	drag coefficient.
d_s, d_p	particle diameter [m].
e_s	restitution coefficient of particle-particle.
e_w	restitution coefficient of wall-particle.
$\vec{g}$	gravity [$m.s^{-2}$].
g_0	radial distribution function.
I_{2D}	second invariant of the deviatoric stress tensor.
C_μ, $C_{1\epsilon}$, $C_{2\epsilon}$, σ_k, σ_ϵ	turbulence model coefficients.
$G_{k,g}$	turbulence kinetic energy production [$kg.m^{-1}.s^{-3}$].
$\bar{\bar{I}}$	unit tensor.
N_c	Courant number.
P_s	solid pressure [$kg.m^{-1}.s^{-2}$].
Re_s	particle Reynolds number.
$\vec{u}$	gas velocity vector [$m.s^{-1}$].
$\vec{v}$	particle velocity vector [$m.s^{-1}$].
$v_{s,slip}$	slip velocity of particle at the wall [$m.s^{-1}$].
$v_{s,w}$	tangential velocity of particle at the wall [$m.s^{-1}$].
N	number of particles.
K	turbulent kinetic energy of gas phase [$m^2.s^{-2}$].
P	pressure [$kg.m^{-1}.s^{-2}$].

Greek letters

Θ	granular temperature [$m^2.s^{-2}$].
$\Pi_{K,g}$, $\Pi_{\epsilon,g}$	influence of the dispersed phases on the continuous phase.
$\mu_{l,g}$	gas molecular viscosity [$kg.m^{-1}.s^{-1}$].
$\mu_{s,col}$	collisional viscosity of solid [$kg.m^{-1}.s^{-1}$].
$\mu_{s,fr}$	frictional viscosity of solid [$kg.m^{-1}.s^{-1}$].
$\mu_{s,kin}$	kinetic viscosity of solid [$kg.m^{-1}.s^{-1}$].
λ_s	bulk viscosity of solid [$kg.m^{-1}.s^{-1}$].
μ_s	shear viscosity of solid [$kg.m^{-1}.s^{-1}$].
$\mu_{t,g}$	gas turbulent viscosity [$kg.m^{-1}.s^{-1}$].
μ_g	gas viscosity [$kg.m^{-1}.s^{-1}$].
Θ_w	granular temperature at wall [$m^2.s^{-2}$].
$\bar{\bar{\tau}}_g$, $\bar{\bar{\tau}}_s$	stress tensor for gas and solid phase respectively [$kg.m^{-1}.s^{-2}$].
$\emptyset_{gs}$	transfer of kinetic energy between phases [$kg.m^{-1}.s^{-3}$].
$k_{\Theta s}$	diffusion coefficient of granular energy [$kg.m^{-1}.s^{-1}$].
$\gamma_{\Theta s}$	collisional energy dissipation [$kg.m^{-1}.s^{-3}$].
$\varepsilon_g, \varepsilon_s$	volume fraction of gas and solid respectively.
$\varepsilon_{s,max}$	maximum packing limit of solids.
ρ_g , ρ_s	gas and solid density [$kg.m^{-3}$].
β	momentum interphase exchange coefficient [$kg.m^{-3}.s^{-1}$].
φ	specularity coefficient.
ϵ	turbulence dissipation energy of gas phase [$m^2.s^{-3}$].

Appendix

Table A1
Governing equations of TFM.

Continuity equations of gas and particulate phase (g for gas and s for particulate).

$$\frac{\partial}{\partial t}(\varepsilon_g.\rho_g) + \left(\nabla.\varepsilon_g.\rho_g.\vec{u}\right) = 0 \quad \text{(A1-1)}$$

$$\frac{\partial}{\partial t}(\varepsilon_s.\rho_s) + (\nabla.\varepsilon_s.\rho_s.\vec{v}) = 0 \quad \text{(A1-2)}$$

Momentum equations of gas and particulate phase.

$$\frac{\partial}{\partial t}(\varepsilon_g.\rho_g.\vec{u}) + \left(\nabla.\varepsilon_g.\rho_g.\vec{u}.\vec{u}\right) = -\varepsilon_g\nabla P - \beta(\vec{u}-\vec{v}) + \nabla.\left(\varepsilon_g.\bar{\bar{\tau}}_g\right) + \varepsilon_g.\rho_g.\vec{g} \quad \text{(A1-3)}$$

$$\frac{\partial}{\partial t}(\varepsilon_s.\rho_s.\vec{v}) + (\nabla.\varepsilon_s.\rho_s.\vec{v}.\vec{v}) = -\varepsilon_s\nabla P - \nabla P_s - \beta(\vec{u}-\vec{v}) + \nabla.(\varepsilon_s.\bar{\bar{\tau}}_s) + \varepsilon_s.\rho_s.\vec{g} \quad \text{(A1-4)}$$

where

$$\bar{\bar{\tau}}_g = \mu_g[\nabla.\vec{u} + (\nabla.\vec{u})^T] - \frac{2}{3}\nabla.\vec{u}\,\bar{\bar{I}} \quad \text{(A1-5)}$$

$$\bar{\bar{\tau}}_s = \mu_s[\nabla.\vec{v} + (\nabla.\vec{v})^T] + \left(\lambda_s - \frac{2}{3}\mu_s\right)\nabla.\vec{v}\,\bar{\bar{I}} \quad \text{(A1-6)}$$

Granular temperature equation.

$$\frac{3}{2}\left[\frac{\partial}{\partial t}\left(\varepsilon_s\rho_s\Theta\right) + \nabla.\left(\varepsilon_s\rho_s\Theta\,\vec{v}\right)\right] = \left(-P_s\,\bar{\bar{I}} + \bar{\bar{\tau}}_s\right):\nabla\vec{v} + \nabla.(k_{\Theta s}\nabla.\Theta) - \gamma_{\Theta s} + \emptyset_{gs} \quad \text{(A1-7)}$$

Table A2
Constitutive correlations of momentum.

Solids pressure [31].	
$P_s = \rho_s \varepsilon_s \Theta + 2g_0 \rho_s \varepsilon^2{}_s \Theta(1+e_s)$	(A2-1)
Solids bulk viscosity [14].	
$\lambda_s = \frac{4}{3}\,\varepsilon_s \rho_s d_p g_0 (1+e_s)\sqrt{\frac{\Theta}{\pi}}$	(A2-2)
Solids shear viscosity.	
$\mu_s = \mu_{s,col} + \mu_{s,kin} + \mu_{s,fr}$	(A2-3)
Collisional viscosity [15].	
$\mu_{s,col} = \frac{4}{5}\,\varepsilon_s{}^2 \rho_s d_p g_0 (1+e_s)\sqrt{\frac{\Theta}{\pi}}$	(A2-4)
Kinetic viscosity [15].	
$\mu_{s,kin} = \frac{10}{96}\sqrt{\Theta\pi}\,\frac{\rho_s d_p}{(1+e_s)g_0}\left[1+\frac{4}{5}g_0\varepsilon_s(1+e_s)\right]^2$	(A2-5)
Frictional viscosity [32].	
$\mu_{s,fr} = \frac{P_s \sin\phi}{\sqrt{4I_{2D}}}$	(A2-6)
Diffusion coefficient of granular energy [15].	
$k_{\Theta s} = 2\,\varepsilon_s{}^2 \rho_s d_p g_0 (1+e_s)\sqrt{\frac{\Theta}{\pi}} + \frac{150\sqrt{\Theta\pi}\rho_s d_p}{384(1+e_s)g_0}\left[1+\frac{6}{5}g_0\varepsilon_s(1+e_s)\right]^2$	(A2-7)
Collisional energy dissipation [31].	
$\gamma_{\Theta s} = 12(1-e_s{}^2)\,\frac{\varepsilon_s{}^2 \rho_s g_0}{d_p\sqrt{\pi}}\Theta^{\frac{3}{2}}$	(A2-8)
Radial distribution function [31].	
$g_0 = \left[1-\left(\frac{\varepsilon_s}{\varepsilon_{s,max}}\right)^{\frac{1}{3}}\right]^{-1}$	(A2-9)
transfer of kinetic energy between phases [15].	
$\emptyset_{gs} = -3\beta\Theta$	(A2-10)
k–ε Turbulence model.	
Gas viscosity.	
$\mu_g = \mu_{l,g} + \mu_{t,g}\,, \qquad \mu_{t,g} = C_\mu \varepsilon_g \rho_g \frac{K}{\epsilon}$	(A2-11)
Turbulance Kinetic energy.	
$\frac{\partial}{\partial t}(\rho_g K) + \nabla.(\rho_g \vec{u} K) = \nabla.\left(\frac{\mu_{t,g}}{\sigma_k}K\right) + G_{k,g} - \rho_g \epsilon + \rho_g \Pi_{k,g}$	(A2-12)
Turbulance dissipation rate.	
$\frac{\partial}{\partial t}(\rho_g \epsilon) + \nabla.(\rho_g \vec{u}\epsilon) = \nabla.\left(\frac{\mu_{t,g}}{\sigma_\epsilon}\epsilon\right) + \frac{\epsilon}{K}(C_{1\epsilon}G_{k,g} - C_{2\epsilon}\rho_g\epsilon) + \rho_g \Pi_{\epsilon,g}$	(A2-13)
where	
$G_{k,g} = \mu_{t,g}(\nabla\vec{u} + (\nabla\vec{u})^T) : \nabla\vec{u}$	(A2-14)
$C_\mu = 0.09,\ C_{1\epsilon} = 1.44,\ \ C_{2\epsilon} = 1.92,\ \sigma_k = 1,\ \sigma_\epsilon = 1.3$	

References

[1] Dahl, S. R. and Hrenya, C. M., "Size segregation in gas-solid fluidized beds with continuous size distributions", *Chem. Eng. Sci.*, **60**, 6658 (2005).

[2] Rasteh, M., Farhadi, F. and Bahramian,

A., "Hydrodynamic characteristics of gas-solid tapered fluidized beds: Experimental studies and empirical models", *Powder Technol.*, **283**, 355 (2015),(DOI:10.1016/j.powtec.2015.06.002).

[3] Chew, J. W., Wolz, J. R. and Hrenya, C. M., "Axial segregation in bubbling gas-fluidized beds with Gaussian and lognormal distributions of Geldart Group B particles", *AIChE J.*, **56**, 3049 (2010).

[4] Joseph, G. G., Leboreiro, J., Hrenya, C. M. and Stevens, A. R., "Experimental segregation profiles in bubbling gas-fluidized beds", *AIChE J.*, **53**, 2804 (2007).

[5] Wu, S. Y. and Baeyens, J., "Segregation by size difference in gas fluidized beds", *Powder Technol.*, **98**, 139 (1998).

[6] Rasul, M. G., Rudolph, V. and Carsky, M., "Segregation potential in binary gas fluidized beds", *Powder Technol.*, **103**, 175 (1999).

[7] Van Wachem, B. G. M., Schouten, J. C., Van den Bleek, C. M., Krishna, R. and Sinclair, J. L., "CFD modeling of gas-fluidized beds with a bimodal particle mixture", *AIChE J.*, **47**, 1292 (2001).

[8] Olivieri, G., Marzocchella, A. and Salatino, P., "A fluid-bed continuous classifier of polydisperse granular solids", *J. Taiwan Inst. Chem. Eng.*, **40**, 638 (2009).

[9] Muzzio, F. J., Shinbrot, T. and Glasser, B. J., "Powder technology in the pharmaceutical industry: The need to catch up fast", *Powder Technol.*, **124**, 1 (2002).

[10] Zhang, Y., Jin, B. and Zhong, W., "Experimental investigation on mixing and segregation behavior of biomass particle in fluidized bed", *Chem. Eng. Process. Process Intensif.*, **48**, 745 (2009).

[11] Zhang, Y., Zhao, Y., Lu, L., Ge, W., Wang, J. and Duan, C., "Assessment of polydisperse drag models for the size segregation in a bubbling fluidized bed using discrete particle method", *Chem. Eng. Sci.*, **160**, 106 (2017).

[12] Chen, X. and Wang, J., "A comparison of two-fluid model, dense discrete particle model and CFD-DEM method for modeling impinging gas–solid flows", *Powder Technol.*, **254**, 94 (2014).

[13] Herzog, N., Schreiber, M., Egbers, C. and Krautz, H. J., "A comparative study of different CFD-codes for numerical simulation of gas–solid fluidized bed hydrodynamics", *Comput. Chem. Eng.*, **39**, 41 (2012).

[14] Huilin, L., Yurong, H., Gidaspow, D., Lidan, Y. and Yukun, Q., "Size segregation of binary mixture of solids in bubbling fluidized beds", *Powder Technol.*, **134**, 86 (2003).

[15] Gidaspow, D., Multiphase flow and fluidization: Continuu and kinetic theory descriptions, Academic Press, (1994).

[16] Cooper, S. and Coronella, C. J., "CFD simulations of particle mixing in a binary fluidized bed", *Powder Technol.*, **151**, 27 (2005).

[17] Huilin, L., Yunhua, Z., Ding, J., Gidaspow, D. and Wei, L., "Investigation of mixing/segregation of mixture particles in gas–solid fluidized beds", *Chem. Eng. Sci.*, **62**, 301 (2007).

[18] Azizi, S., Hosseini, S. H., Ahmadi, G. and Moraveji, M., "Numerical simulation of particle segregation in bubbling gas-fluidized beds", *Chem. Eng. Technol.*, **33**, 421 (2010).

[19] Chao, Z., Wang, Y., Jakobsen, J. P.,

Fernandino, M. and Jakobsen, H. A., "Multi-fluid modeling of density segregation in a dense binary fluidized bed", *Particuology*, **10**, 62 (2012).

[20] Formisani, B., Girimonte, R. and Longo, T., "The fluidization pattern of density-segregating binary mixtures", *Chem. Eng. Res. Des.*, **86**, 344 (2008).

[21] Geng, S., Jia, Z., Zhan, J., Liu, X. and Xu, G., "CFD modeling the hydrodynamics of binary particle mixture in pseudo-2D bubbling fluidized bed: Effect of model parameters", *Powder Technol.*, **302**, 384 (2016).

[22] Feng, Y. Q., Xu, B. H., Zhang, S. J., Yu, A. B. and Zulli, P., "Discrete particle simulation of gas fluidization of particle mixtures", *AIChE J.*, **50**, 1713 (2004).

[23] Norouzi, H. R., Mostoufi, N. and Sotudeh-Gharebagh, R., "Effect of fines on segregation of binary mixtures in gas–solid fluidized beds", *Powder Technol.*, **225**, 7 (2012).

[24] Schaafsma, S. H., Marx, T. and Hoffmann, A. C, "Investigation of the particle flowpattern and segregation in tapered fluidized bed granulators", *Chem. Eng. Sci.*, **61**, 4467 (2006).

[25] Zhang, Y., Zhong, W., Jin, B. and Xiao, R., "Mixing and segregation behavior in a spout-fluid bed: Effect of particle size", *Ind. Eng. Chem. Res.*, **51**, 14247 (2012).

[26] Santos, K. G., Francisquetti, M. C. C., Malagoni, R. A. and Barrozo, M. A. S., "Fluid dynamic behavior in a spouted bed with binary mixtures differing in size", *Dry. Technol.*, **33**, 1746 (2015).

[27] Johnson, P. C. and Jackson, R., "Frictional–collisional constitutive relations for granular materials, with application to plane shearing", *J. Fluid Mech.*, **176**, 67 (1987).

[28] Li, T., Grace, J. and Bi, X., "Study of wall boundary condition in numerical simulations of bubbling fluidized beds", *Powder Technol.*, **203**, 447 (2010).

[29] Bahramian, A., Olazar, M. and Ahmadi, G., "Effect of slip boundary conditions on the simulation of microparticle velocity fields in a conical fluidized bed", *AIChE J.*, **59**, 4502 (2013).

[30] Zhang, Y., Zhao, Y., Lu, L., Ge, W., Wang, J. and Duan, C., "Assessment of polydisperse drag models for the size segregation in a bubbling fluidized bed using discrete particle method", *Chem. Eng. Sci.*, **160**, 106 (2017).

[31] Lun, C. K. K., Savage, S. B., Jeffrey, D. J. and Chepurniy, N., "Kinetic theories for granular flow: Inelastic particles in Couette flow and slightly inelastic particles in a general flowfield", *J. Fluid Mech.*, **140**, 223 (1984).

[32] Schaeffer, D. G., "Instability in the evolution equations describing incompressible granular flow", *J. Differ. Equ.*, **66**, 19 (1987).